# Factors Controlling Cage Escape Yields of Closed and Open Shell Metal Complexes in Bimolecular Photoinduced Electron Transfer

Alexia Ripak,[‡] Ana Karem Vega Salgado,[‡] Danillo Valverde,[†] Silvia Cristofaro,[†] Alban de Gary,[†] Yo-ann Olivier,[†]* Benjamin Elias[‡]* and Ludovic Troian-Gautier[‡,ϕ]*

[‡] UCLouvain, Institut de la Matière Condensée et des Nanosciences (IMCN), Molecular Chemistry, Materials and Catalysis (MOST), Place Louis Pasteur 1/L4.01.02, B-1348 Louvain-la-Neuve, Belgium

[†]Laboratory for Computational Modeling of Functional Materials, Namur Institute of Structured Matter, University of Namur, Rue de Bruxelles 61, 5000 Namur, Belgium.

[ϕ]Wel Research Institute, Avenue Pasteur 6, 1300 Wavre, Belgium

*KEYWORDS. Cage escape Yields • Iron • Ruthenium • Iridium*

**ABSTRACT:** The cage escape yield, *i.e*. the separation of the geminate radical pair formed immediately after bimolecular excited-state electron transfer was studied in eleven solvents using six Fe(III), Ru(II), Os(II) and Ir(III) photosensitizers and tri-*p*-tolylamine as the electron donor. Among all complexes, the largest cage escape yields (0.67-1) were recorded for the Ir(III) photosensitizer showing the highest potential as a photocatalyst in photoredox catalysis. These yields dropped to values around 0.65 for both Ru(II) photosensitizers and to values around 0.38 for the Os(II) photosensitizer. Interestingly, for both open shell Fe(III) complexes, the yields were small (<0.1) in solvents with dielectric constants greater than 20 but were shown to reach values up to 0.58 in solvents with low dielectric constant. The results presented herein on closed shell photosensitizers suggest that the low rate of triplet-singlet intersystem crossing within the manifold of states of the geminate radical pair implies that charge recombination towards the ground state is a spin forbidden process, favoring large cage escape yields that are not influenced by dielectric effects. Geminate charge recombination in open-shell metal complexes, such as the two Fe(III) photosensitizers studied herein, is no longer a spin forbidden process and becomes highly sensitive to solvent effects. Altogether, this study provides general guidelines for factors influencing bimolecular excited-state reactivity using prototypical photosensitizers but also allows to foresee a great development of Fe(III) photosensitizers with $^2$LMCT excited state in photoredox catalysis, providing that solvent with low dielectric constants are used.

## INTRODUCTION

The cage escape concept was first introduced in 1934 by Franck and Rabinowitsch while studying the photochemical generation of radicals in solution. Molecules that populate dissociative excited states were used, leading to a corresponding geminate radical pair upon homolytic bond cleavage.[1-2] Franck and Rabinowitsch initially proposed that the geminate products had to possess sufficient kinetic energy to "*find their way through the surrounding 'walls' of the solvent and to put more molecular layers between them before coming to rest*".[2] Experimental evidence of this cage effect was provided by Lyon and Levy, who investigated the decomposition of mixtures of azomethane and per-deuterated azomethane in the gas phase and in isooctane solutions.[3] In the gas phase, a 1:2:1 statistical distribution of $CH_3CH_3$, $CH_3CD_3$ and $CD_3CD_3$ was obtained, respectively. However, in isooctane solutions, the photolysis yielded almost exclusively the in-cage recombination products, *i.e.* $CH_3CH_3$ and $CD_3CD_3$. These crossover experiments provided one of the first experimental evidence that solvent molecules trapped the reactive radicals, preventing their escape, and thus influencing product distribution as indicated by the quantitative yield for radical homocoupling.

The cage escape yield ($\Phi_{CE}$) has also attracted much interest in the field of photoredox catalysis where it is used to describe the separation of the geminate radical pair formed upon the bimolecular electron transfer reactivity between an excited-state photosensitizer and a quencher.[4] Historically, cage escape yields have been extensively studied with organic photosensitizers such as cyano-substituted anthracene, as well as pyrylium, xanthene and perylene derivatives.[5-12] With respect to transition metal photosensitizers, most reported studies have centered around the oxidative quenching of $[Ru(bpy)_3]^{2+}$ by methyl viologen derivatives.[13-17] There, cage escape yields often ranged between 0.2 and 0.4, on average. Recently there has been a regained interest in fundamental studies related to the determination and understanding of cage escape yields.[18-23] As such, increased yields for oxidative quenching of Ru(II) and Ir(III) derivatives were recently reported using aryl diazonium derivatives.[23-24] In cases where the driving force for electron transfer was large, these yields even reached unitary values. Reductive quenching of organic and transition metal photosensitizers has also been reported. In most cases, the cage escape yields for the reaction between transition metal photosensitizers were larger than for oxidative quenching.

The factors that impact cage escape yields are not yet well-defined, and several studies have investigated these yields[25] with respect to the solvent polarity and viscosity,[26-30] the driving force for electron transfer,[31-32] the spin states[27-28, 33-36] as well as

ionic strength effects.[29-30, 33, 37] Pioneers in the field have dedicated tremendous resources to the understanding of cage escape in the 1970s and 1990s, but unfortunately, no conclusive, overarching mechanism has been reached to date.

Additionally, research dedicated to this fundamental phenomenon was reduced, presumably for research dedicated to the development of applications. It is therefore of tremendous importance to study these cage escape processes and provide insight into the parameters that control these yields.

A revigorated interest in cage escape yields came from the demonstration that they could impact the overall reaction yields of light-induced transformations. Although intuitive, this was verified experimentally for the light induced dehalogenation reaction using $[Fe(phtmeimb)_2]^+$,[19-20, 38] a luminescent iron(III) photosensitizer pioneered by Wärnmark and co-workers.[39] High reaction yields were obtained in conditions where $\Phi_{CE}$ were greater than 0.3, while small yields were obtained when $\Phi_{CE}$ dropped below 0.10.[19] Similar observations were recently made by Wenger and co-workers while comparing Ru(II) and Cr(III) photosensitizers.[40]

In here, we report a systematic study of $\Phi_{CE}$ for metal complexes photosensitizers exhibiting lower-lying excited states with different natures and spin multiplicities. We selected one Os(II) and two Ru(II) photosensitizers with triplet metal-to-ligand charge transfer ($^3$MLCT) excited states, two Fe(III) complexes with doublet ligand-to-metal charge transfer ($^2$LMCT) excited states and one Ir(III) photosensitizer with a mixed $^3$MLCT and triplet ligand-centered ($^3$LC) excited state (**Figure 1**). The photosensitizers were reductively quenched by tri-*p*-tolylamine (TTA) in eleven solvents. Overall, it was shown that $\Phi_{CE}$ were almost solvent invariant when excited states with triplet character were considered, and followed the trend Os(II)<Ru(II)<Ir(III). $\Phi_{CE}$ were large for Ir(III) with values around 0.67-1 and reached values around 0.65 for the Ru(II) photosensitizers and 0.38 for the Os(II) photosensitizers. Interestingly, for both Fe(III) photosensitizers, $\Phi_{CE}$ were small (<0.10) in solvents with dielectric constants greater than 20 but reached large values (between 0.17 and 0.58) when the dielectric constant was smaller than 11.

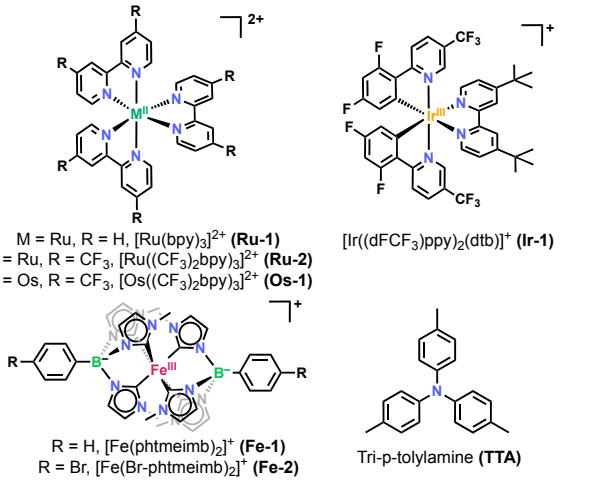


**Figure 1. Structures of the photosensitizers and quencher used in this work. All photosensitizers have $PF_6^-$ counter-ions.**

## RESULTS AND DISCUSSION

The structures of TTA and the six photosensitizers are shown in **Figure 1**. $[Fe(phtmeimb)_2]^+$ (**Fe-1**), $[Fe(Br\text{-}phtmeimb)_2]^+$ (**Fe-2**), $[Ru(bpy)_3]^{2+}$ (**Ru-1**), $[Ru((CF_3)_2bpy)_3]^{2+}$ (**Ru-2**), $[Os((CF_3)_2bpy)_3]^{2+}$ (**Os-1**) and $Ir(dFCF_3)ppy)_2(dtb)]^+$ (**Ir-1**) absorbed visible light with appreciable molar absorption coefficients (**Figure 2a**). Their important photophysical and electrochemical properties are gathered in **Table 1**. The Ru(II) and Ir(III) photosensitizers had excited-state lifetimes that were in the microsecond range, whereas much shorter excited-state lifetime were determined for **Os-1** (63 ns) and both Fe(III) photosensitizers (2 ns).

**Table 1. Photophysical and electrochemical properties of the photosensitizers**

| PS | τ (Ar, $CH_3CN$) [ns] | $E_{red}$[a] [V vs NHE] | $E^*_{red}$[a] [V vs NHE] |
|---|---|---|---|
| **Fe-1** | 2 | –0.56 | +1.63 |
| **Fe-2** | 2 | –0.51 | +1.58 |
| **Os-1** | 63 | –0.50 | +1.31 |
| **Ru-1** | 890 | –1.10 | +1.10 |
| **Ru-2** | 1510 | –0.62 | +1.54 |
| **Ir-1** | 2010 | –1.13 | +1.45 |

[a]Recorded in acetonitrile containing 0.1M $TBAPF_6$.

**Table 2. Quenching rate constants ($k_q$) for the excited-state quenching of the different photosensitizers by TTA in the indicated solvents.**

| Solvent | $k_q$ ($x10^{10}M^{-1}s^{-1}$) | | | | | |
|---|---|---|---|---|---|---|
| | Fe-1 | Fe-2 | Os-1 | Ru-1 | Ru-2 | Ir-1 |
| **$CHCl_3$** | 1.71 | 1.36 | N.S | Ins. | Ins. | 1.21 |
| **Glyme** | 1.1 | 1.1 | 0.031 | 0.001 | 0.22 | 1.87 |
| **THF** | 1.22 | 1.23 | Ins. | Ins. | 0.17 | 1.09 |
| **$CH_2Cl_2$** | 2.5 | 2.4 | N.S | 0.13 | 0.39 | 1.27 |
| **$PhCF_3$** | 1.78 | 1.71 | Ins. | Ins. | Ins. | 0.90 |
| **DCE** | 1.66 | 1.47 | 0.12 | 0.17 | 0.16 | 0.89 |
| **BuCN** | 1.47 | 1.49 | 0.049 | 0.043 | 0.38 | 0.91 |
| **Acetone** | 2.03 | 2.05 | 0.049 | 0.035 | 0.33 | 1.31 |
| **PropCN** | 1.64 | 1.54 | 0.064 | 0.050 | 0.28 | 0.24 |
| **$CH_3CN$** | 0.63 | 0.69 | 0.083 | 0.085 | 0.64 | 1.1 |
| **DMSO** | 0.61 | 0.69 | 0.006 | 0.007 | 0.098 | 0.28 |

Ins = Insoluble, N. S. : not stable throughout the experiment.

The excited-state quenching of the six photosensitizers with TTA ($E°(TTA^{\bullet+/0})$ = 1.07 V vs NHE in $CH_3CN$) was investigated in eleven solvents: chloroform ($CHCl_3$), glyme, tetrahydrofuran (THF), dichloromethane ($CH_2Cl_2$), α,α,α-trifluorotoluene ($PhCF_3$), dichloroethane (DCE), butyronitrile (BuCN), acetone, propionitrile (PropCN), acetonitrile ($CH_3CN$) and dimethylsulfoxide (DMSO). Even if bulk solvent properties and local environments of the solvent cage might be very different, the dielectric constant (ε) was selected as the main descriptor for comparison and discussion purposes. A range in ε that covers the scale between 4.6 ($CHCl_3$) and 46.7 (DMSO) was used. A representative example of excited-state quenching of **Ir-1** by TTA in dichloromethane is shown in **Figure 2b**. The photoluminescence decay at each concentration of quencher was analyzed according to the Stern-Volmer equation which provided a linear correlation (inset of **Figure 2b**) from which the Stern-

Volmer constant ($K_{SV}$) could be determined. The quenching rate constant ($k_q$) was then determined by dividing $K_{SV}$ by the excited-state lifetime in the absence of quencher. In almost all cases, large quenching rate constants, near the diffusion limit, were determined, in line with the favorable driving force for electron transfer. In the case of **Ru-1** and **Os-1**, the driving force for electron transfer was moderate, which is evidenced by the moderate quenching rate constants in some solvents. The quenching rate constants were systematically smaller in DMSO, in agreement with the greater viscosity of DMSO compared to the other solvents. The quenching rate constants for all photosensitizers are tabulated in **Table 2**.

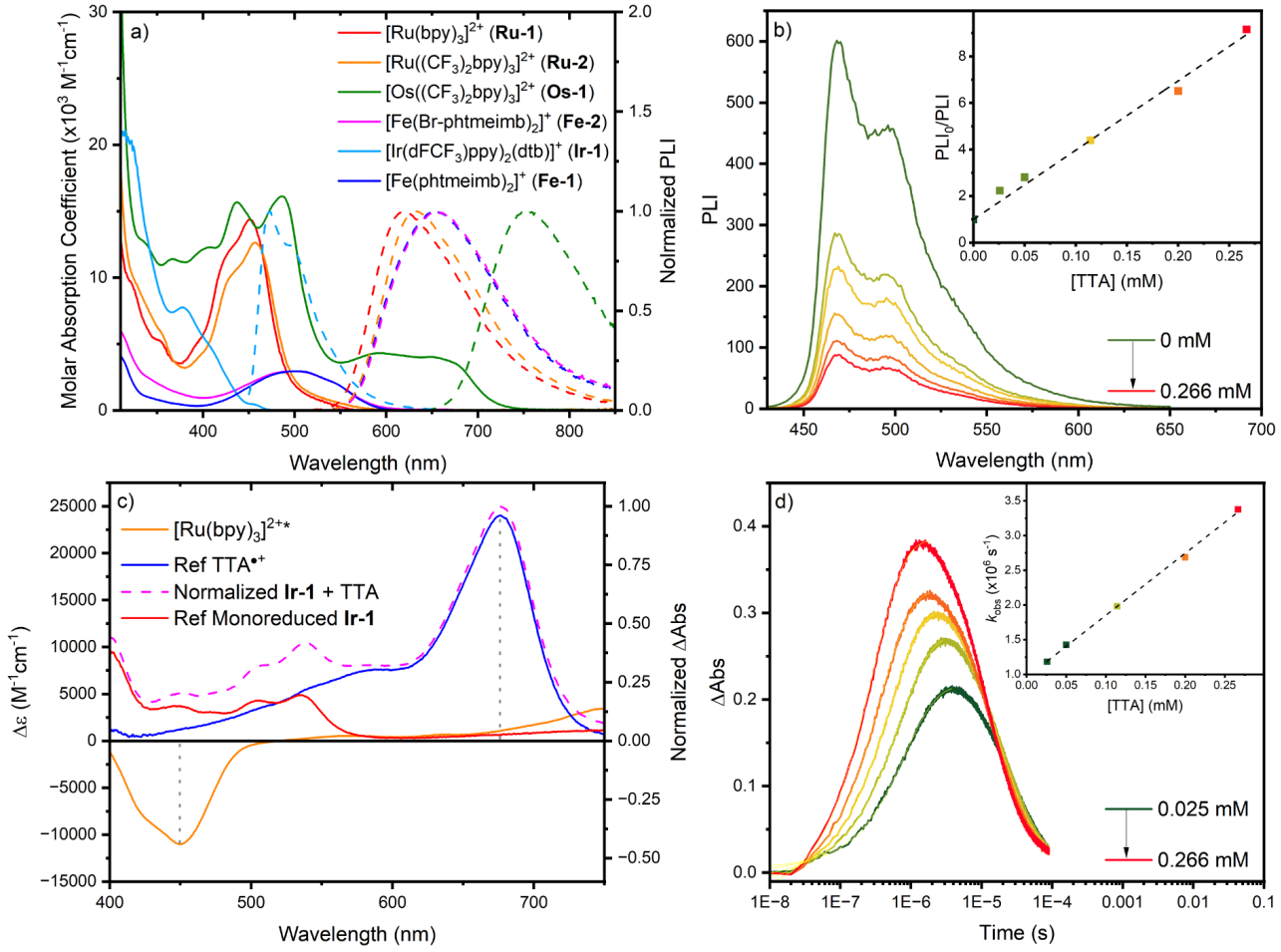


**Figure 2. a) UV-Visible absorption spectra (solid) and steady-state photoluminescence spectra (dashed) of the six photosensitizers in acetonitrile. b) Steady-state photoluminescence quenching of Ir-1 by TTA in argon purged dichloromethane. The inset represents the Stern-Volmer plot from which the quenching rate constant, $k_q$ = 1.27 x10$^{10}$ M$^{-1}$s$^{-1}$ was determined. c) Nanosecond transient absorption spectra of the $[Ru(bpy)_3]^{2+}$ actinometer (orange), as well as the reaction between Ir-1 and TTA following pulsed 420 nm light excitation (magenta dashed line) in argon purged acetonitrile. Reference spectra of monoreduced Ir-1 (red) and TTA$^{\bullet+}$ (blue) are presented as well. d) Single wavelength absorption changes recorded at 670 nm following pulsed 420 nm light excitation of Ir-1 in the presence of increasing amounts of TTA in dichloromethane. The growth of the single wavelength absorption changes was fit (yellow overlaid line) and used to determine the electron transfer rate constant, $k_{et}$ = 8.9 x10$^9$ M$^{-1}$s$^{-1}$ (inset).**

Excited-state electron transfer from TTA to the excited photosensitizer was confirmed by nanosecond transient absorption spectroscopy for all six photosensitizers with the unambiguous observation of the oxidized TTA$^{\bullet+}$ radical cation with an absorption maximum around 670 nm and the corresponding reduced photosensitizer (**Figure 2c**). For **Ir-1**, **Ru-1** and **Ru-2**, the growth of the signal at 670 nm corresponding to TTA$^{\bullet+}$ could be well time-resolved and was thus used to determine the corresponding electron transfer rate constants that agreed with the quenching rate constants determined via Stern-Volmer analysis (**Figure 2d** and **Table S1**).

We then turned to the determination of $\Phi_{CE}$ by comparative actinometry using Eq. 1 and 2 with $[Ru(bpy)_3]^{2+}$ as actinometer.[24]

$$\Phi_{CE} = \frac{\Phi}{\%\ PL\ Quenched} \qquad \text{Eq. 1}$$

$$\Phi = \left( \frac{\frac{\Delta A_{PS^-}}{\Delta \varepsilon_{PS^-}}}{\frac{\Delta A_{ES_{ref}}}{\Delta \varepsilon_{ES_{ref}}}} \right) \left( \frac{1-10^{-Abs_{ref}(\lambda_{exc})}}{1-10^{-Abs_{PS}(\lambda_{exc})}} \right) \qquad \text{Eq. 2}$$

From Eq. 1, $\Phi_{CE}$ are obtained by comparing the relative yield of mono-oxidized TTA$^{\bullet+}$ or mono-reduced PS produced ($\Phi$) to the percentage of quenched PL (%PL). The relative yield of photoproducts ($\Phi$) is determined through Eq. 2, where $\Delta A$ is the change in absorbance of mono-oxidized TTA$^{\bullet+}$ or mono-reduced PS, $\Delta\varepsilon$ is the change in molar absorption coefficient and Abs is the absorbance value at the irradiation wavelength. These signals were compared to the changes in absorption of the

reference $[Ru(bpy)_3]^{2+}$ ($ES_{ref}$) at 450nm. A Δε value of –11000 $M^{-1}cm^{-1}$ was used for the actinometer at 450 nm.[41-43]

We mention that the determination of cage escape yields is highly sensitive to the magnitude of the parameters described above. The values of these parameters are often obtained via steady-state or transient absorption spectroscopy, and specifically, Δε values are usually determined by spectroelectrochemistry in one solvent. We concluded that the use of the literature value of $\Delta\varepsilon_{670nm}$ = 25,000 $M^{-1}cm^{-1}$ for $TTA^{\bullet+}$ in all solvents led to unphysical results with $\Phi_{CE}$ values between 0.9 and 1.5 for **Ir-1**. $\Phi_{CE}$ larger than 1 would imply that one encounter could lead to more than 1 equivalent of product which does not have a physical meaning for a bimolecular reaction unless a propagation mechanism takes place, which is not the case here. Thus, the molar absorption coefficient of $TTA^{\bullet+}$ was determined in most solvents, either by chemical oxidation or by spectroelectrochemistry in the presence of 0.1 M *tetra-n*-butylammonium hexafluorophosphate ($TBAPF_6$). Several chemical oxidants were used, namely $NOBF_4$, $Cu(ClO_4)_2$, Cerium ammonium nitrate ($[Ce(NO_3)_6](NH_4)_2$) and antimony pentachloride ($SbCl_5$). The combination of chemical oxidation and spectroelectrochemistry was used to ascertain that the 0.1M electrolyte used in electrochemistry did not significantly impact the molar absorption coefficient (**Figures S63-S71**). In acetonitrile, the chemical oxidation using $NOBF_4$, the spectra of isolated $TTA^{\bullet+}BF_4$ or $TTA^{\bullet+}SbCl_6$ as well as spectroelectrochemistry led to almost identical values in all cases, *i.e.* 25,500 $M^{-1}cm^{-1}$. Strikingly, in dichloromethane, the change in molar absorption coefficient was much larger (34,500 $M^{-1}cm^{-1}$ on average) when determined by chemical oxidation or spectroelectrochemistry. Overall, this two-pronged approach resulted in molar absorption coefficients in the 25,500 to 34,500 $M^{-1}cm^{-1}$ range (**Table 3**). Unfortunately, it was not possible to apply this methodology in all solvents due to either side reactions or a spectral overlap between the first and second oxidation wave of tri-*p*-tolylamine. Thus, for these solvents, a value identical to the one determined in $CH_3CN$ was used.

With these newly determined molar absorption coefficients, we turned to nanosecond transient absorption to determine the corresponding cage escape yields. The changes were monitored at 670 nm, *i.e.* at or close to the maximum absorption changes corresponding to the oxidized tri-*p*-tolylamine cation ($TTA^{\bullet+}$). A representative example for the bimolecular excited-state electron transfer between **Ir-1** and TTA in dichloromethane is presented in **Figure 2d**, while all $\Phi_{CE}$ are gathered in **Figure 3**, **Table 3** and **Figures S1-S62**.

Among the closed-shell photosensitizers, **Ir-1** was the photosensitizer with the largest cage escape yields that ranged from 0.67-0.84 in dichloromethane to 1 in most of the solvents. These very large values are in line with **Ir-1** being one of the most effective photosensitizers for photoredox catalysis applications.[23, 44-51] **Ru-1** and **Ru-2** presented solubility issues in some apolar solvents and we did not attempt to circumvent these limitations by changing the counter-ions for consistency. Nevertheless $\Phi_{CE}$ were smaller than those determined with **Ir-1** and ranged from 0.41 to 0.87 for **Ru-1** and from 0.50 to 0.77 for **Ru-2**, respectively. **Ru-1** provided almost consistently cage escape yields that were slightly larger than **Ru-2**, *i.e.* an average $\Phi_{CE}$ of 0.68 for **Ru-1** and an average $\Phi_{CE}$ of 0.60 for **Ru-2**.

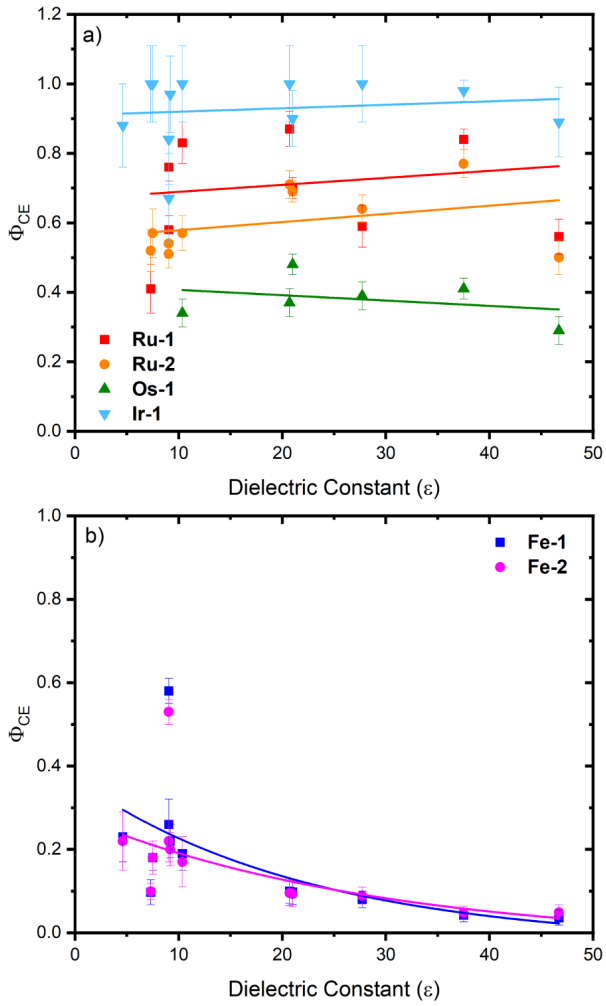


**Figure 3. Cage escape yields for Ir-1, Ru-1, Ru-2 and Os-1 (a) as well as for Fe-1 and Fe-2 (b) in different solvents. A linear fit (a) and an exponential fit (b) are added to guide the eye.**

Assuming similar reorganization energy (λ) in line with the computed values (*vide infra*), a larger difference in cage escape yields might have been expected based on Marcus theory. Indeed, a recent study proposed that larger cage escape yields are obtained when the geminate charge recombination is located further into the Marcus inverted region.[40] As the geminate charge recombination is not a photo-induced reaction, the driving force is simply determined as the difference in electric potential of the two substances that are involved, i.e. the reduced photosensitizer and the oxidized donor. Thus, based on the redox potential gathered in **Table 1** and $E(TTA^{\bullet+/0})$ = 1.07 V vs NHE, $\Delta G_{gcr}$ can be determined as –1.57, –2.17,–1.69 and –2.2 V vs NHE for **Os-1**, **Ru-1**, **Ru-2** and **Ir-1**, respectively. **Ru-1** is located 510 mV and 630 mV further into the Marcus inverted region than **Ru-2** and **Os-1** respectively which should have led to a bigger difference in cage escape yields. For **Os-1**, cage escape yields were significantly smaller than those determined with the other Ru(II) or Ir(III) photosensitizers, ranging from 0.29 to 0.48, despite the fact that they could only be determined in solvents with a dielectric constant greater than 10 due to solubility and stability issues. Assuming a reorganization of 1eV, **Os-1** and **Ru-2** have similar driving force for geminate charge recombination, yet the cage escape yields vary drastically. Finally, **Ru-1** and **Ir-1** have the largest $\Delta G_{gcr}$ and also exhibit the

largest cage escape yields. However, the cage escape yields are systematically larger for **Ir-1** than for **Ru-1**. As such, it does not appear, using this series of closed-shell photosensitizers, that the driving force for geminate charge recombination is the main contributor in the first place to cage escape yields.

Both **Fe-1** and **Fe-2** are open-shell photosensitizers and exhibit similar properties in terms of excited-state lifetimes and ground and excited-state redox potentials. Initially, it was envisioned that the introduction of a Br substituent would lead to partial state mixing within the geminate radical pair, thereby conferring some spin-forbidden character to the geminate charge recombination and thus increasing $\Phi_{CE}$. This hypothesis was shown as incorrect as the $\Phi_{CE}$ were not significantly different between **Fe-1** and **Fe-2**. The cage escape yields ranged from 0.036 in DMSO to 0.56 in dichloromethane eluted over basic alumina to remove potential traces of HCl.[52] $\Phi_{CE}$ gradually increased with the decreased dielectric constant of the solvent, with a sharp increase observed for dielectric constant values below 11 (**Figure 3**).[53]

**Table 3. Cage Escape Yields for the indicated solvents-photosensitizers combinations.**

| Solvent | e | η (cP) | Δε ($M^{-1}cm^{-1}$) | $\Phi_{ce}$ | | | | | |
|---|---|---|---|---|---|---|---|---|---|
| A | | | | Fe-1 | Fe-2 | Os-1 | Ru-1 | Ru-2 | Ir-1 |
| **$CHCl_3$** | 4.6 | 0.54 | 33,000 | 0.23 | 0.22 | N.S | Ins. | Ins. | 0.94 |
| **Glyme** | 7.3 | 0.46 | ---[c] | 0.097 | 0.099 | -- | 0.41 | 0.52 | 1 |
| **THF** | 7.5 | 0.50 | ---[c] | 0.18 | 0.18 | Ins | Ins. | 0.57 | 1 |
| **$CH_2Cl_2$** | 9.0 | 0.44 | 34,500 | 0.26 | 0.22 | N.S. | 0.76 | 0.54 | 0.67 |
| **$CH_2Cl_2$[a]** | 9.0 | 0.44 | 34,500 | 0.58 | 0.53 | N.S | 0.58 | 0.51 | 0.84 |
| **$PhCF_3$** | 9.2 | 0.47 | 27,000 | 0.22[b] | 0.20[b] | Ins | Ins. | Ins. | 0.97 |
| **DCE** | 10.4 | 0.78 | 29,500 | 0.19 | 0.17 | 0.42 | 0.83 | 0.57 | 1 |
| **BuCN** | 20.7 | 0.60 | ---[c] | 0.10 | 0.095 | 0.38 | 0.87 | 0.71 | 1 |
| **Acetone** | 21 | 0.36 | 25,500 | 0.098 | 0.093 | 0.41 | 0.70 | 0.69 | 0.90 |
| **PropCN** | 27.7 | 0.44 | ---[c] | 0.08 | 0.089 | 0.41 | 0.59 | 0.64 | 1 |
| **$CH_3CN$** | 37.5 | 0.38 | 25,500 | 0.03 | 0.04 | 0.38 | 0.84 | 0.77 | 0.98 |
| **DMSO** | 46.7 | 1.99 | ---[c] | 0.02 | 0.036 | 0.11 | 0.56 | 0.50 | 0.89 |

[a]$CH_2Cl_2$ first eluted through basic $Al_2O_3$. See text for additional details. [b]A pre-solubilization in acetonitrile (less than 0.1%) was required for $PhCF_3$. Since $CH_3CN$ gives poor $\Phi_{CE}$, the value obtained are mostly due to $PhCF_3$ solvation. [c]Could not be determined by spectroelectrochemistry or chemical oxidation and as such, a value identical to the one determined in acetonitrile was used. Ins = Insoluble, N. S. : not stable throughout the experiment.

Density Functional Theory (DFT) and its time-dependent version (TD-DFT) framework were used to describe the electronic structure of **Ru-1**, **Ru-2**, **Os-1**, **Ir-1** and **Fe-1** as well as TTA in gas and solvent phases ($CHCl_3$ and DMSO). Solvation effects were included via conductor version of the polarizable continuum model (CPCM).[54] Ground and excited state minima were optimized by employing the hybrid B3LYP functional within the zero-order regular approximation (ZORA)[55] to consider relativistic effects. The def2-TZVP basis set for all the lighter elements and a specific basis set (SARC-ZORA-TZVP) for metal atoms were used. Spin-orbit couplings (SOC) between singlet and triplet states were also computed at the same level of the geometry optimizations. All QM calculations were performed using the ORCA 5.0.4 program.[56]

The electronic nature of the lowest singlet ($S_1$) and triplet ($T_1$) excited states in their respective optimized geometry was assigned through a fragment-based analysis of the transition density matrix, as implemented in TheoDORE 3.1.1 package,[57] in gas phase (**Figure S72**) and in two different solvents (results obtained in $CHCl_3$ and DMSO are shown in **Figure 4** and **S73**, respectively) for the Ru, Ir and Os photosensitizers. For **Ru-1**, **Ru-2** and **Os-1**, the bar plots of **Figure 4** highlight the strong MLCT character (green bars) of $S_1$ and $T_1$ excited states. In contrast, **Ir-1** compound exhibits a mixed LLCT/MLCT and LC/MLCT character for the $S_1$ and $T_1$ states, respectively, in agreement with the literature.[58] Hole-electron density plots (upper panel of **Figures 4** and **S72-73**) further confirm the MLCT character of **Ru-1**, **Ru-2** and **Os-1** due to the pronounced localization of the electron on one of the symmetrically equivalent ligands and of the hole on the metal center, respectively. Analogously, the hybrid LC/MLCT $T_1$ character of **Ir-1** is also detectable in the hole-electron density plot, in which a large hole density is centered on one of the two ppy ligands rather than on the metal core, whereas the electron density is localized on the lone ppy ligand. Additionally, the mixed LLCT/MLCT character is confirmed by the delocalization of the hole distribution on the metal center and the ppy ligand. Along with the aforementioned analysis, the active role played by the metal in the CT excited states is also observed by computing the SOC between $S_1$ and $T_1$ states of the metal complexes. We calculated large SOC (see **Table S2**) up to 6.3 meV for both **Ru-1** and **Ru-2** and 17 meV for **Os-1** (at least one order of magnitude larger than the commonly computed SOC of organic compounds),[59] due to the involvement of the *d* orbitals of the metals. Even though Ir has a higher nuclear charge compared to Ru, lower SOC values of 2.7 and 1.2 in $CHCl_3$ and DMSO, respectively, were computed for the **Ir-1** photosensitizer, which are consistent with the lower contribution of the metal atom in the $S_1$ and $T_1$ electronic excitation as compared to the other closed-shell complexes. While the characterization of the encounter complex is essentially defined by the nature of the excited states of the photosensitizers alone, the investigation of the geminate radical pair of both the reduced ($PS^{\bullet-}$) and oxidized ($Q^{\bullet+}$) species needs to be taken into account. As a preliminary step, we optimized the

geometry of the PS and Q separately in their reduced and oxidized states, at the DFT level, using the same level of theory described in this section. We then computed the internal reorganization energy ($\lambda_i$) associated with the geminate charge recombination from the reduced/oxidized state of the photosensitizer/quencher to the ground state ({$PS^{\bullet-}$;$Q^{\bullet+}$}→ {PS; Q}). As expected, in the case of electron transfer, we obtained significantly smaller values of $\lambda_i$ compared to the dominating reorganization energy coming from solvent contribution ($\lambda_s$), usually around 1 eV.[60-64] Indeed, $\lambda_i$ values in the gas phase are in the range of 0.2-0.3 eV for **Fe-1**, **Ru-2**, **Os-1,** and **Ir-1** and lower than 0.1 eV for **Ru-1** and TTA, for which minor geometric changes are observed (see **Figure S75**). As a second step, we calculated the ground-state minimum structures of the PS-Q complex using the B3LYP functional, including D4 semiempirical dispersion correction[65] for which an equilibrium distance between the central nitrogen atom of TTA and the metal atom of the PS in the range of 7-8 Å was found. TD-DFT calculations carried out on top of the optimized geometries showed that the energetically most stable singlet and triplet excited states exhibit a strong CT character that mimics the electronic configuration of the geminate radical pair. The rate associated with the geminate charge recombination process regenerating the ground state of the PS and the Q competes with the diffusional process allowing the ionized species to escape from the solvent cage and thus leading to cage escape. However, the geminate charge recombination towards the ground state must be a spin-conserving process such as the reverse intersystem crossing (RISC) rate from the triplet geminate radical pair state ($^3$[$PS^{\bullet-}$ $Q^{\bullet+}$]) to the singlet one ($^1$[$PS^{-}Q^{+}$]) has to be non-negligible. Interestingly, all the investigated PS-Q complexes lead to almost degenerate $^3$[$PS^{\bullet-}Q^{\bullet+}$] and $^1$[$PS^{-}Q^{+}$] states displaying both a strong CT behavior (see **Table S7**).

We explored the magnitude of the couplings mediating the RISC process leading to a spin flip, namely SOC and the hyperfine coupling (HFC). In line with El-Sayed's rule that forbids ISC between electronic states of similar electronic nature, *e.g.* CT states, the computed SOC was found to be small and in the order of $\mu$eV (values are reported in **Table S3**) with moderately larger values for the **Os-1** complex. An even minor contribution of one order of magnitude lower than the intermolecular SOC (see **Table S6**) was disclosed for the HFC. As described in the work of Gillet *et al.*,[66] a singlet-triplet gap in the order of 1-3 meV (see **Table S7**) is actually too large to render the spin state interconversion rate driven by HFC a competitive process. However, we cannot exclude that such a mechanism would not be contributing for more distant configuration of the PS and the Q where the singlet-triplet energy gap would be even smaller. Finally, we computed the electronic coupling associated with the back electron transfer process using the Q-Chem 5.4 software[67] (see section 6 in the SI for more details), which falls into the meV range or below with a slightly larger value for the **Os-1** complex.

Altogether, these results suggest that the lower cage escape yield for **Os-1** would originate from a larger SOC between singlet and the triplet states of the geminate radical pair which would favor geminate charge recombination to the ground state.

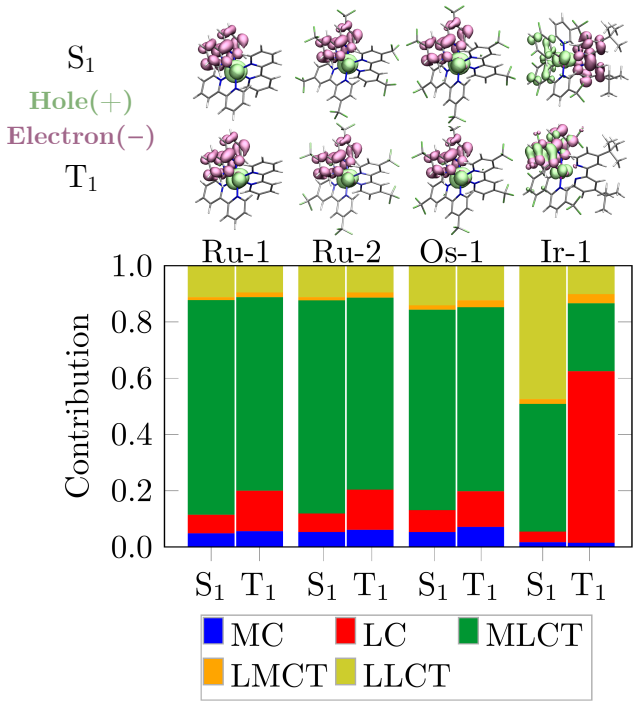


**Figure 4. Top panel: Hole-electron density plots of the $S_1$ (first row) and the $T_1$ (second row) computed in their corresponding optimized minimum structure for Ru-1, Ru-2, Os-1, and Ir-1 in $CHCl_3$, where the pink and the green regions represent the electron and the hole distributions, respectively. Hole-electron density plots in the gas phase and in DMSO are shown in the SI since almost identical results are obtained for Ru-1, Ru-2, and Os-1 compared to $CHCl_3$. Bottom panel: bar plots describing the CT (MLCT (green), LLCT (yellow), and LMCT(orange)) and the LE (MC (blue) and LC (red)) contributions to the character of the $S_1$ and $T_1$ excited states in their optimized geometry: the MLCT is strongly predominant in both $S_1$ and $T_1$ for Ru-1, Ru-2, and Os-1, whereas for Ir-1 it is predicted a mixed LC/MLCT in $S_1$ and LLCT/MLCT in $T_1$, respectively. In analogy with the hole-electron plots, we only reported the results in $CHCl_3$. Gas phase and DMSO bar plots are given in the SI.**

***Origin of these cage escape yields.*** The results presented herein offer a unique opportunity to gauge the relative impact of solvent, the spin multiplicity of the relevant states involved or competing with the cage escape, spin orbit coupling, steric bulk, driving force and dipole moment orientation on cage escape yields. From the results, it appears that for **Ru-1**, **Ru-2**, **Os-1** and **Ir-1**, the spin multiplicity of the geminate radical pair is a triplet (although it could also exist as a singlet state) largely favored by the spin conserved electron transfer from the triplet encounter complex suggesting that the spin of the excited state of the metal complex is an important contributor to $\Phi_{CE}$. This was proposed, amongst others, in a seminal paper by Olmsted and Meyer that showed that cage escape yields were drastically increased when an anthracene energy shuttle was used as energy acceptor from $[Ru(bpy)_3]^{2+}$, thus generating a pure triplet anthracene that reacted with methylviologen.[17] These experiments were carried out in controlled solutions and provided evidence that the difference in spin between the geminate radical (namely a triplet) and the ground state (namely a singlet state) was an important factor that rendered the geminate charge recombination spin-forbidden, thus increasing $\Phi_{CE}$. However, it should be noted that the energy transfer from the photosensitizer to the

energy shuttle also changed the driving force for electron transfer itself, which could have impacted the cage escape yields as well. The results presented herein support that the spin of the relevant states involved in the cage escape being a key contributor to its overall yield. When considering the photosensitizers with $^3$MLCT excited states, *i.e.* **Os-1**, **Ru-1** and **Ru-2**, the cage escape yields are overall smaller for **Os-1** than for **Ru-1** and **Ru-2**. Although these three photosensitizers exhibit $^3$MLCT excited states, the larger SOC of **Os-1** in the geminate radical pair as suggested by the calculations (see **Table S3**), compared to **Ru-1** and **Ru-2** could render the in-cage geminate charge recombination less spin forbidden (**Figure 4**). Indeed, RISC would be enhanced in **Os-1** leading to a non-negligible population of the singlet geminate radical pair state. The differences in $\Phi_{CE}$ between **Ru-1** and **Ru-2** were small, and as such there does not seem to be a drastic effect from steric bulk in these tris-homoleptic photosensitizers. This observation might be different in heteroleptic complexes. It should also be noted that **Os-1** and **Ru-2** offer similar driving force for geminate charge recombination in view of their similar reduction potential (see **Table 1**), yet the $\Phi_{CE}$ are significantly smaller for **Os-1**. As such, it appears that the driving force for geminate charge recombination is not a key contributor to the cage escape for photosensitizers with marked triplet character.

Interestingly, the yields were consistently larger for the Ir(III) photosensitizer, which is expected to have a SOC as large as the Os(II) photosensitizers. However, the triplet excited state of **Ir-1** is characterized by a combination of $^3$LC and $^3$MLCT character[58, 68] and as such, with less contribution from the d-orbital in **Ir-1** and increased π-orbital contributions, SOC between $S_1$ and $T_1$ compared to **Ru-1**, **Ru-2** and **Os-1** as confirmed by TD-DFT calculations (see **Table S2**). Within the geminate radical pair, the SOC computed for the {**Ir-1**;TTA} was smaller than for {**Os-1**;TTA} but comparable to {**Ru-1**;TTA} and {**Ru-2**;TTA} (**Table S3**). This suggests that the reverse ISC would be on the same order of magnitude for the Ru(II) and Ir(III) photosensitizers but smaller than for **Os-1**.

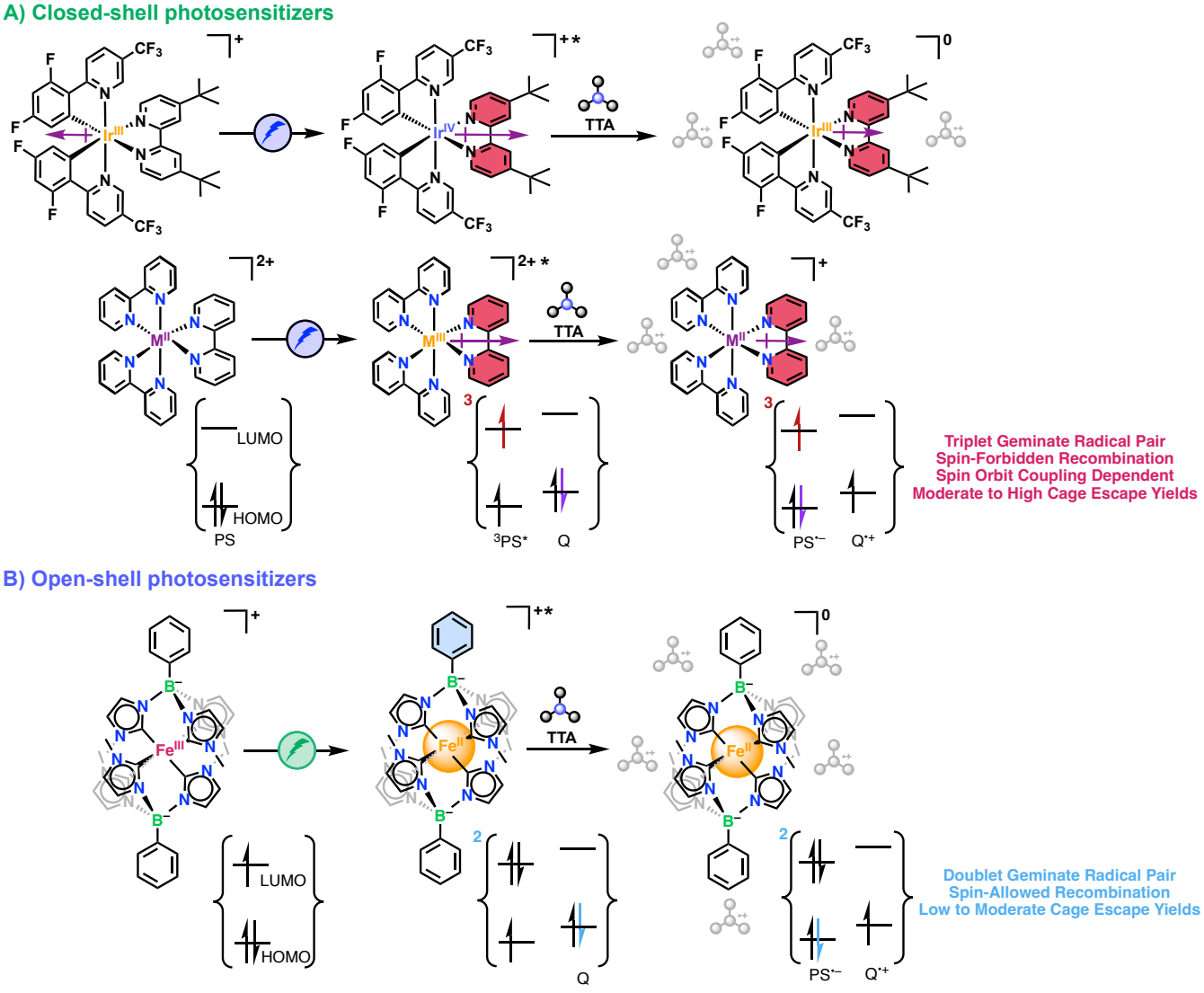


**Figure 5. Potential difference in reactivity for closed-shell and open-shell photosensitizers. For closed-shell photosensitizers, the dipole of the reduced state is directed from the metal to the reduced ligand. In the case of open-shell photosensitizers with LMCT excited states, the metal center is formally reduced, which creates a dipole change different than closed-shell photosensitizers. Charge recombination to the TTA$^{\bullet+}$ (grey structures) involves different orbitals when closed-shell and open-shell photosensitizers. The electronic configuration of the photosensitizer and geminate radical pair is presented within the backets.**

The lower $\Phi_{CE}$ obtained for Fe(III) photosensitizers can in part also be explained by their spin. Indeed, **Fe-1** and **Fe-2** display $^2$LMCT excited states (see Figure S74). Hence, upon excited-state electron transfer, this generates a radical pair where in-cage geminate charge recombination is spin allowed (**Figure 5**), thus decreasing the cage escape yields. However, the trend observed with dielectric constant, with values that ranged from 0.036 in DMSO to 0.58 in dichloromethane suggested that other parameters are important. We had initially proposed that, in halogenated solvents, increased ISC and/or state mixing within the geminate radical pair might take place using **Fe-1**.[19] The results obtained with **Fe-2** bearing Br groups, in addition to the relatively large cage escape yields obtained in THF and trifluorotoluene suggested that such increased state mixing did not take place. However, a solvent with a small dielectric constant might increase the electrostatic repulsion between the reduced iron photosensitizers and $TTA^{\bullet+}$. The excited-state electron transfer is termed a "charge-shift reaction", in which both the reactants and products have a total plus one charge and hence no net Coulombic work term contribution is expected.[69-70] However, given the structure of **Fe-1** and **Fe-2**, it could be that local polarization would be more prominent in solvent with lower dielectric constant, hence creating an electric field that would assist separation of the electron transfer products. This was also previously suggested[19] and could account for the increased yields observed for **Fe-1** and **Fe-2** in dichloromethane. It should however be noted that such effects have not been observed with **Ru-1**, **Ru-2** or **Os-1**, which should have experienced greater repulsion in solvents with low dielectric constant than **Fe-1** and **Fe-2**. In addition, the reaction with **Ir-1** is also a "charge-shift reaction" and such effects were also not observed. Thus, it appears that spin of the excited state or within the geminate pair represents a main contributor to the cage escape yields, and that electrostatic repulsion is more prominent for photosensitizers where in-cage geminate charge recombination is spin allowed.

The discussion on the electrostatic interaction within the geminate radical pair as well as the impact of solvent effects on its relative energy to the ground state can be supported by a discussion on the change of the electrical dipole moment magnitude orientation of the different metal complexes in the different states that they would occupy before cage escape takes place. In **Ir-1**, the excited state dipole is directed from the metal center to the 4,4'-$(tBu)_2$-2,2'-bipyridine ligand (**Figure S79)**. Upon reduction by TTA, the dipole moment is still oriented in the same direction but significantly reduced (1.8 D for $PS^-$ and 10.1 D in $T_1$ in $CHCl_3$, similar trends are observed in DMSO). This efficiently creates a directionality of the electron transfer process and could impact the geometry of the encounter complex, making the back electron transfer less favorable if the oxidized $TTA^{\bullet+}$ is located in the less bulky region, at the opposite side of the bulky ligand. The scenario would be different for homoleptic and symmetric **Os-1**, **Ru-1** and **Ru-2** photosensitizers since a reduction in dipole moment between the excited and reduced state is observed while their orientation in both states are parallel (see **Table S8** and Figures **S76-78**), thus leading to a still possibly favored geminate charge recombination. Note that the change in dipole moment with respect to the ground state for the $^3$MLCT state of **Ru-1** has been determined by Stark spectroscopy as being slightly larger than for $[Os(bpy)_3]^{2+}$, 4.0 D *vs* 3.4 D.[71] The change in dipole moment for **Ru-2** has been determined as 8.3 D.[72] The calculations predicts a larger change of electrical dipoles overall, but the dipoles in $T_1$ is larger for **Ru-2** than for **Ru-1** similarly as in the experiments. In the case of **Fe-1** and **Fe-2**, a very small change in dipole moment in the excited state is expected for symmetry reasons. Upon reduction, the electrical dipole moment barely changes so that there is no net change of electrical dipole moment for both complexes. In addition, due to symmetry, most of the geometries of the encounter complex around the metal center would become equivalent. The main difference in this scenario comes from the localization of the electron involved in the geminate charge recombination reaction. For **Ir-1**, **Os-1**, **Ru-1** and **Ru-2**, this electron is localized in π orbitals located on the 2,2'-bipyridine type ligand, whereas for **Fe-1** and **Fe-2**, the electron is located on the $d^6$ metal orbitals. To some extent, this is reminiscent of the prototypical oxidative electron transfer between a Ru(II) photosensitizer and methyl viologen, (where charge recombination involves the metal-centered d orbitals) that operates with cage escape yields that are much smaller than those determined for reductive electron transfer.[13-17] As such, the small cage escape yields determined for iron photosensitizers could originate from the orbitals involved in the geminate charge recombination process, coupled with electrostatic repulsion afforded by the low dielectric solvents.

## CONCLUSIONS

In conclusion, the excited-state electron transfer and $\Phi_{CE}$ were quantified in 11 solvents for the reaction between six Fe(III), Ru(II), Os(II) and Ir(III) photosensitizers and TTA. The reaction proceeded via reductive excited-state electron transfer to generate the reduced photosensitizer and the oxidized quencher, $TTA^{\bullet+}$. The cage escape yields, *i.e.* the separation of the reduced photosensitizer and the oxidized quencher within the geminate radical pair were the largest for **Ir-1**, that reached an average value of 0.93 in 11 solvents. These large $\Phi_{CE}$ are probably responsible for the wide use of **Ir-1** in photoredox catalysis. $\Phi_{CE}$ using **Ru-1** and **Ru-2** were smaller than those determined with **Ir-1** but still reached appreciable values around 0.65, while Os(II) exhibited lower values around 0.38. With these Os(II), Ru(II) and Ir(III) photosensitizers, there did not seem to be any trend with bulk solvent properties such as the dielectric constant or solvent viscosity, for example. Only the two iron photosensitizers exhibited some degree of correlation with the dielectric constant, as $\Phi_{CE}$ gradually increased as the dielectric constant of the solvent decreased. Overall, the results presented herein do not allow to develop a complete theory for $\Phi_{CE}$ but offer some general conclusions and guidelines for the use of these photosensitizers in light-mediated transformations:

- *The overall spin multiplicity of the photosensitizer is key in order to maximize the cage escape yield:* There are clearly two families of photosensitizers that arise: the closed-shell and the open-shell ones. On the closed-shell photosensitizers, we observed that the dominant triplet character of the geminate radical pair intrinsically limits geminate charge recombination to the ground state, which is a singlet state. Open-shell photosensitizers entail that the spin multiplicity of all the involved electronic states (including the ground state) is of the same spin multiplicity (*i.e.* doublet). The process competing with cage escape, namely geminate charge recombination from the geminate radical pair directly generated from the encounter complex state, is *de facto* a spin-conserved process which could occur on faster timescale.

- *The magnitude of the (reverse) intersystem crossing within the geminate radical pair is a key elementary process influencing cage escape yield of closed-shell photosensitizers:* **Ir-1**, which displays a marked $^3$LC character, exhibited larger cage escape yields than the other photosensitizers. **Os-1**, with its larger SOC value, mixed triplet and singlet state more efficiently than their Ru(II) and Ir(III) counterparts, and thus produced smaller cage escape yields.
- *The driving force for geminate charge recombination ($\Delta G_{gcr}$) is not the main factor influencing the cage escape yields.* For closed-shell photosensitizers, this is intimately related to the previous point. Assuming that the spin conversion within the geminate radical is the limiting process, charge recombination does not appear to be a major factor involved in the kinetics of cage escape even though the energy difference between the geminate radical pair and the ground state is expected to be highly dependent on dielectric effects caused by varying the solvent. A further proof of this argument comes from the carefully selected series of photosensitizers where several compounds show almost identical $\Delta G_{gcr}$, yet $\Phi_{CE}$ vary drastically. Several trends with $\Delta G_{gcr}$ have been reported in the literature and as such, we hypothesize that SOC, leading to the triplet-singlet spin flip, dominates $\Delta G_{gcr}$ in the Ru(II), Os(II) and Ir(III) series.
- *The orbitals involved in the geminate charge recombination could be of importance:* Herein the recombination occurred from an electron localized in π-orbitals of the ligand for **Os-1**, **Ru-1**, **Ru-2** and **Ir-1**, or from d$^6$ metal orbitals in the case of **Fe-1** and **Fe-2**. As such, both recombination scenarios might be associated with different electronic coupling constants, further impacting $\Phi_{CE}$.
- Other factors might also contribute: As the role of the dipole moment changes involved in the geminate charge recombination process cannot be ruled out.

Further studies are currently underway to attempt to disentangle the relative contribution of each parameter but, altogether, the data presented herein does provide novel insight into the use of these photosensitizers for photoredox catalysis. For example, whereas a plethora of solvent might be used for Ir(III) photosensitizers, it does seem that only solvent with a dielectric constant lower than ~15 would actually be useful if Fe(III) photosensitizer were to be used. We believe that these kind of studies are of paramount importance to render light-induced processes more efficient and could open the door to the further development of earth abundant photosensitizers based on Fe(II/III), Cr(III) or Mo(0), for example.

## ASSOCIATED CONTENT

### Supporting Information

The Supporting Information is available free of charge on the ACS Publications website.

## AUTHOR INFORMATION


### Corresponding Author

Ludovic.Troian@uclouvain.be
Benjamin.Elias@uclouvain.be
Yoann.Olivier@unamur.be


### Author Contributions

The manuscript was written through contributions of all authors. All authors have given approval to the final version of the manuscript.


### Funding Sources

Grant no. 23/28-135 (L.T.-G, B.E. and Y.O.).
Grant no. U.N021.21 (B.E.).
grant no. 40020332 (L.T.-G)

## ACKNOWLEDGMENT

This work was supported by the "Action de Recherche Concertée" through the project "UNCAGED" under grant no. 23/28-135. This work was supported by the Fonds de la Recherche Scientifique (F.R.S.-FNRS) under grant no. U.N021.21 (B.E.) and CDR grant nº. 40020332 (L.T.-G.). L.T.-G. is a Chercheur Qualifié of the Fonds de la Recherche Scientifique – FNRS. A. R. thanks the Belgian National Funds for Scientific Research (F.R.S.-FNRS) for their Fund for Research Training in Industry and Agriculture (FRIA) PhD grant. A.R., B.E. and L.T.-G. gratefully acknowledge the UCLouvain for financial support. D. V., S. C., and Y. O. acknowledge funding from Fonds de la Recherche Scientifique-FNRS under grant No. F.4534.21. This research used resources of the "Plateforme Technologique de Calcul Intensif (PTCI)" (http://ww.ptci.unamur.be) located at the university of Namur, Belgium, which is supported by the FNRS-FRFC, the Walloon Region, and the University of Namur (Conventions No. 2.5020.11, GEQ U.G006. 15, 1610468, RW/GEQ2016 et U.G011.22). The PTCI is member of the "Consortium des Equipements de Calcul Intensif (CECI)" (http://ww.ceci-hpc.be). The present research benefited from the computational resources made available on Lucia, the Tier-1supercomputer of the Wallon Region, infrastructure funded by the Walloon Region under the grant agreement n° 1910247.



## KEYWORDS

Cage escape Yields; Iron; Ruthenium; Iridium; Osmium.


## REFERENCES


1. Kornfeld, G.; Farkas, L.; Rabinowitsch, E., General Discussion. *Trans. Faraday Soc.* **1934,** *30*, 130-131.
2. Franck, J.; Rabinowitsch, E., Some Remarks About Free Radicals and the Photochemistry of Solutions. *Trans. Faraday Soc.* **1934,** *30*, 120-130.
3. Lyon, R. K.; Levy, D. H., Demonstration of the "Cage" Effect. *J. Am. Chem. Soc.* **1961,** *83*, 4290-4290.
4. De Kreijger, S.; Gillard, M.; Elias, B.; Troian-Gautier, L., Spectroscopic Techniques to Unravel Mechanistic Details in Light-Induced Transformations and Photoredox Catalysis. *ChemCatChem* **2024,** *16*, e202301100.
5. Niwa, T.; Kikuchi, K.; Matsusita, N.; Hayashi, M.; Katagiri, T.; Takahashi, Y.; Miyashi, T., Solvent Effects on Photoinduced Electron-Transfer Reactions. *J. Phys. Chem* **1993,** *97*, 11960-11964.
6. Gould, I. R.; Ege, D.; Moser, J. E.; Farid, S., Efficiencies of Photoinduced Electron-Transfer Reactions: Role of the Marcus Inverted Region in Return Electron Transfer within Geminate Radical-Ion Pairs. *J. Am. Chem. Soc.* **1990,** *112*, 4290-4301.
7. Lewis, F. D.; Bedell, A. M.; Dykstra, R. E.; Elbert, J. E.; Gould, I. R.; Farid, S., Photochemical Generation, Isomerization, and Oxygenation of Stilbene Cation Radicals. *J. Am. Chem. Soc.* **1990,** *112*, 8055-8064.
8. Jayanthi, S. S.; Ramamurthy, P., Excited Singlet State Reactions of Thiopyrylium with Electron Donors: Electron Transfer, Induction of Triplet by Internal and External Heavy Atom Effect, and Comparison of Pyrylium and Thiopyrylium Reactions. *J. Phys. Chem. A* **1998,** *102*, 511-518.
9. S. Jayanthi, S.; Ramamurthy, P., Photoinduced Electron Transfer Reactions of 2,4,6-Triphenylpyrylium: Solvent Effect and

Charge-Shift Type of Systems. *Phys. Chem. Chem. Phys.* **1999,** *1*, 4751-4757.

10. Klimtchuk, E. S.; Irinyi, G.; Khudyakov, I. V.; Margulis, L. A.; Kuzmin, V. A., Effect of Magnetic Field on Radical Yields During the Photoreduction of Xanthene Dyes in Viscous Media. *J. Chem. Soc., Faraday Trans. 1* **1989,** *85*, 4119-4128.

11. Douglas, P.; Waechter, G.; Mills, A., Ionic Srength Effects on the Ground State Complexation and Triplet State Electron Transfer Reaction between Rose Bengall and Methyl Viologen. *Photochem. Photobiol.* **1990,** *52*, 473-479.

12. Iwa, P.; Steiner, U. E.; Vogelmann, E.; Kramer, H. E. A., Linear Free-Enthalpy Relation for Radical Yield in Fluorescence Quenching by Electron Transfer. *J. Phys. Chem* **1982,** *86*, 1277-1285.

13. Hoffman, M. Z., Cage Escape Yields from the Quenching of Excited Tris(Bipyridyl)Ruthenium(2+) by Methylviologen in Aqueous Solution. *J. Phys. Chem* **1988,** *92*, 3458-3464.

14. Sun, H.; Yoshimura, A.; Hoffman, M. Z., Oxidative Quenching of the Excited State of Tris(2,2'-Bipyridine)Ruthenium(2+) Ion by Methylviologen. Variation of Solution Medium and Temperature. *J. Phys. Chem* **1994,** *98*, 5058-5064.

15. Clark, C. D.; Hoffman, M. Z., Ion-Pairing Control of Excited-State Electron-Transfer Reactions. Quenching, Charge Recombination, and Back Electron Transfer. *J. Phys. Chem* **1996,** *100*, 7526-7532.

16. Clark, C. D.; Hoffman, M. Z., Ion-Pairing Control of Excited-State Electron-Transfer Reactions Effect of Cations on Cationic Reactants. *J. Photoch. Photobio. A* **1997,** *111*, 9-13.

17. Olmsted, J.; Meyer, T. J., Factors Affecting Cage Escape Yields Following Electron-Transfer Quenching. *J. Phys. Chem* **1987,** *91*, 1649-1655.

18. Sittel, S.; Sell, A. C.; Hofmann, K.; Wiedemann, C.; Nau, J. P.; Kerzig, C.; Manolikakes, G.; Heinze, K., Visible-Light Induced Fixation of So2 into Organic Molecules with Polypyridine Chromium(Iii) Complexes. *ChemCatChem* **2023,** *15*, e202201562.

19. Aydogan, A.; Bangle, R. E.; Cadranel, A.; Turlington, M. D.; Conroy, D. T.; Cauët, E.; Singleton, M. L.; Meyer, G. J.; Sampaio, R. N.; Elias, B.; Troian-Gautier, L., Accessing Photoredox Transformations with an Iron(Iii) Photosensitizer and Green Light. *J. Am. Chem. Soc.* **2021,** *143*, 15661-15673.

20. Aydogan, A.; Bangle, R. E.; De Kreijger, S.; Dickenson, J. C.; Singleton, M. L.; Cauët, E.; Cadranel, A.; Meyer, G. J.; Elias, B.; Sampaio, R. N.; Troian-Gautier, L., Mechanistic Investigation of a Visible Light Mediated Dehalogenation/Cyclisation Reaction Using Iron(Iii), Iridium(Iii) and Ruthenium(Ii) Photosensitizers. *Catal. Sci. Technol.* **2021,** *11*, 8037-8051.

21. Bürgin, T. H.; Glaser, F.; Wenger, O. S., Shedding Light on the Oxidizing Properties of Spin-Flip Excited States in a Criii Polypyridine Complex and Their Use in Photoredox Catalysis. *J. Am. Chem. Soc.* **2022,** *144*, 14181-14194.

22. Sinha, N.; Wegeberg, C.; Häussinger, D.; Prescimone, A.; Wenger, O. S., Photoredox-Active Cr(0) Luminophores Featuring Photophysical Properties Competitive with Ru(Ii) and Os(Ii) Complexes. *Nature Chem.* **2023,** *155*, 1730-1736.

23. Ripak, A.; De Kreijger, S.; Sampaio, R. N.; Vincent, C. A.; Cauët, É.; Jabin, I.; Tambar, U. K.; Elias, B.; Troian-Gautier, L., Photosensitized Activation of Diazonium Derivatives for C–B Bond Formation. *Chem Catal.* **2023,** *3*, 100490.

24. Ripak, A.; De Kreijger, S.; Elias, B.; Troian-Gautier, L., A Protocol for Determining Cage-Escape Yields Using Nanosecond Transient Absorption Spectroscopy. *STAR Protocols* **2023,** *4*, 102312.

25. Goodwin, M. J.; Dickenson, J. C.; Ripak, A.; Deetz, A. M.; McCarthy, J. S.; Meyer, G. J.; Troian-Gautier, L., Factors That Impact Photochemical Cage Escape Yields. *Chem. Rev.* **2024,** *124*, 7379-7464.

26. Jayanthi, S.; Ramamurthy, P., Photoinduced Electron Transfer Reactions of 2,4,6 Triphenylpyrylium: Solvent Effect and Charge-Shift Type of Systems. *Phys. Chem. Chem. Phys.* **1999,** *1*, 4751-4757.

27. Aydogan, A.; Bangle, R. E.; Cadranel, A.; Turlington, M. D.; Conroy, D. T.; Cauët, E.; Singleton, M. L.; Meyer, G. J.; Sampaio, R. N.; Elias, B.; Troian-Gautier, L., Accessing Photoredox Transformations with an Iron(Iii) Photosensitizer and Green Light. *J. Am. Chem. Soc.* **2021,** *143*, 15661-15673.

28. Wolff, H.-J.; Bürßner, D.; Steiner, U. E., Spin-Orbit Coupling Controlled Spin Chemistry of $Ru(Bpy)_3^{2+}$ Photooxidation: Detection of Strong Viscosity Dependence of in-Cage Backward Electron Transfer Rate. *Pure Appl. Chem.* **1995,** *67*, 167-174.

29. Meidlar, K.; Das, P. K., Tris(2,2'-Bipyridine)Ruthenium(Ii)-Sensitized Photooxidation of Phenols. Environmental Effects on Electron Transfer Yields and Kinetics. *J. Am. Chem. Soc.* **1982,** *104*, 7462-7469.

30. Ohno, T.; Lichtin, N. N., Electron Transfer in the Quenching of Triplet Methylene Blue by Complexes of Iron(Ii). *J. Am. Chem. Soc.* **1980,** *102*, 4636-4643.

31. Sun, H.; Neshvad, G.; Hoffman, M. Z., Energy Gap Dependence of the Efficiency of Charge Separation Upon the Sacrificial Reductive Quenching of the Excited States of Ru(Ii)-Diimine Photosensitizers in Aqueous Solution. *Mol. Cryst. Liq. Cryst.* **2006,** *194*, 141-150.

32. DiLuzio, S.; Connell, T. U.; Mdluli, V.; Kowalewski, J. F.; Bernhard, S., Understanding Ir(Iii) Photocatalyst Structure-Activity Relationships: A Highly Parallelized Study of Light-Driven Metal Reduction Processes. *J. Am. Chem. Soc.* **2022,** *144*, 1431-1444.

33. Hoffman, M. Z., Cage Escape Yields from the Quenching of $*Ru(Bpy)_3^{2+}$ by Methylviologen in Aqueous Solution. *J. Phys. Chem.* **1988,** *92*, 3458–3464.

34. Gibbons, D. J.; Farawar, A.; Mazzella, P.; Leroy-Lhez, S.; Williams, R. M., Making Triplets from Photo-Generated Charges: Observations, Mechanisms and Theory. *Photochem. Photobiol. Sci.* **2020,** *19*, 136-158.

35. Olmsted III, J.; Meyer, T. J., Factors Affecting Cage Escape Yields Following Electron-Transfer Quenching. *J. Phys. Chem.* **1987,** *91*, 1649–1655.

36. Kikuchi, K.; Hoshi, M.; Niwa, T.; Takahashi, Y.; Miyashi, T., Heavy-Atom Effects on the Excited Singlet-State Electron-Transfer Reaction. *J. Phys. Chem.* **1991,** *95*, 38–42.

37. Kalyanasundaram, K.; Neumann-Spallart, M., Influence of Added Salts on the Cage Escape Yields in the Photoredox Quenching of $Ru(Bpy)_2^{+3}$ Excited States. *Chem. Phys. Lett.* **1982,** *88*, 7-12

38. Glaser, F.; Aydogan, A.; Elias, B.; Troian-Gautier, L., The Great Strides of Iron Photosensitizers for Contemporary Organic Photoredox Catalysis: On Our Way to the Holy Grail? *Coord. Chem. Rev.* **2024,** *500*, 215522.

39. Kjær, K. S.; Kaul, N.; Prakash, O.; Chábera, P.; Rosemann, N. W.; Honarfar, A.; Gordivska, O.; Fredin, L. A.; Bergquist, K.-E.; Häggström, L*., et al.*, Luminescence and Reactivity of a Charge-Transfer Excited Iron Complex with Nanosecond Lifetime. *Science* **2019,** *363*, 249-253.

40. Wang, C.; Li, H.; Bürgin, T. H.; Wenger, O. S., Cage Escape Governs Photoredox Reaction Rates and Quantum Yields. *Nature Chem.* **2024**.

41. Yoshimura, A.; Hoffman, M. Z.; Sun, H., An Evaluation of the Excited State Absorption Spectrum of Ru(Bpy)32+ in Aqueous and Acetonitrile Solutions. *J. Photoch. Photobio. A* **1993,** *70*, 29-33.

42. Goez, M.; von Ramin-Marro, D.; Othman Musa, M. H.; Schiewek, M., Photoionization of [Ru(Bpy)3]2+: A Catalytic Cycle with Water as Sacrificial Donor. *J. Phys. Chem. A* **2004,** *108*, 1090-1100.

43. Müller, P.; Brettel, K., [Ru(Bpy)3]2+ as a Reference in Transient Absorption Spectroscopy: Differential Absorption Coefficients for Formation of the Long-Lived 3mlct Excited State. *Photochem. Photobio. Sci.* **2012,** *11*, 632-636.

44. Wang, C.-S.; Dixneuf, P. H.; Soulé, J.-F., Photoredox Catalysis for Building C–C Bonds from C(Sp2)–H Bonds. *Chem. Rev.* **2018,** *118*, 7532-7585.

45. Tay, N. E. S.; Lehnherr, D.; Rovis, T., Photons or Electrons? A Critical Comparison of Electrochemistry and Photoredox Catalysis for Organic Synthesis. *Chem. Rev.* **2022,** *122*, 2487-2649.

46. Narayanam, J. M. R.; Stephenson, C. R. J., Visible Light Photoredox Catalysis: Applications in Organic Synthesis. *Chem. Soc. Rev.* **2011,** *40*, 102-113.

47. Glaser, F.; Wenger, O. S., Recent Progress in the Development of Transition-Metal Based Photoredox Catalysts. *Coord. Chem. Rev.* **2020,** *405*, 213129.
48. Earley, J. D.; Zieleniewska, A.; Ripberger, H. H.; Shin, N. Y.; Lazorski, M. S.; Mast, Z. J.; Sayre, H. J.; McCusker, J. K.; Scholes, G. D.; Knowles, R. R*., et al.*, Ion-Pair Reorganization Regulates Reactivity in Photoredox Catalysts. *Nature Chem.* **2022,** *14*, 746-753.
49. Chan, A. Y.; Perry, I. B.; Bissonnette, N. B.; Buksh, B. F.; Edwards, G. A.; Frye, L. I.; Garry, O. L.; Lavagnino, M. N.; Li, B. X.; Liang, Y*., et al.*, Metallaphotoredox: The Merger of Photoredox and Transition Metal Catalysis. *Chem. Rev.* **2022,** *122*, 1485-1542.
50. Xu, B.; Troian-Gautier, L.; Dykstra, R.; Martin, R. T.; Gutierrez, O.; Tambar, U. K., Photocatalyzed Diastereoselective Isomerization of Cinnamyl Chlorides to Cyclopropanes. *J. Am. Chem. Soc.* **2020,** *142*, 6206-6215.
51. Morton, C. M.; Zhu, Q.; Ripberger, H.; Troian-Gautier, L.; Toa, Z. S. D.; Knowles, R. R.; Alexanian, E. J., C–H Alkylation Via Multisite-Proton-Coupled Electron Transfer of an Aliphatic C–H Bond. *J. Am. Chem. Soc.* **2019,** *141*, 13253-13260.
52. Armarego, W. L. F., Chapter 4 - Purification of Inorganic and Metal-Organic Chemicals. In *Purification of Laboratory Chemicals (Eighth Edition)*, Armarego, W. L. F., Ed. Butterworth-Heinemann: 2017; pp 635-770.
53. Note that the values reported in dichloromethane are different from the one initially reported. This is due the value of Δε for the actinometer. In the present study, we used a value of –11000 $M^{-1}cm^{-1}$ while previous reports have used a value of –15000 $M^{-1}cm^{-1}$.
54. Barone, V.; Cossi, M., Quantum Calculation of Molecular Energies and Energy Gradients in Solution by a Conductor Solvent Model. *J. Phys. Chem. A* **1998,** *102*, 1995-2001.
55. van Lenthe, E.; Snijders, J. G.; Baerends, E. J., The Zero-Order Regular Approximation for Relativistic Effects: The Effect of Spin–Orbit Coupling in Closed Shell Molecules. *J. Chem. Phys.* **1996,** *105*, 6505-6516.
56. Neese, F., The Orca Program System. *WIREs Computational Molecular Science* **2012,** *2*, 73-78.
57. Plasser, F., Theodore: A Toolbox for a Detailed and Automated Analysis of Electronic Excited State Computations. *J. Chem. Phys.* **2020,** *152*, 084108.
58. Singh, A.; Teegardin, K.; Kelly, M.; Prasad, K. S.; Krishnan, S.; Weaver, J. D., Facile Synthesis and Complete Characterization of Homoleptic and Heteroleptic Cyclometalated Iridium(Iii) Complexes for Photocatalysis. *J. Organomet. Chem.* **2015,** *776*, 51-59.
59. Olivier, Y.; Yurash, B.; Muccioli, L.; D'Avino, G.; Mikhnenko, O.; Sancho-García, J. C.; Adachi, C.; Nguyen, T. Q.; Beljonne, D., Nature of the Singlet and Triplet Excitations Mediating Thermally Activated Delayed Fluorescence. *Phys. Rev. Mater.* **2017,** *1*, 075602.
60. Place, I.; Farran, A.; Deshayes, K.; Piotrowiak, P., Triplet Energy Transfer through the Walls of Hemicarcerands: Temperature Dependence and the Role of Internal Reorganization Energy. *J. Am. Chem. Soc.* **1998,** *120*, 12626-12633.
61. Moser, C. C.; Chobot, S. E.; Page, C. C.; Dutton, P. L., Distance Metrics for Heme Protein Electron Tunneling. *Biochim. Biophys. Acta Bioenerg.* **2008,** *1777*, 1032-1037.
62. Dutton, P. L.; Mosser, C. C., Quantum Biomechanics of Long-Range Electron Transfer in Protein: Hydrogen Bonds and Reorganization Energies. *Proc. Natl. Acad. Sci. USA* **1994,** *91*, 10247-10250.
63. Reynolds, L.; Gardecki, J. A.; Frankland, S. J. V.; Horng, M. L.; Maroncelli, M., Dipole Solvation in Nondipolar Solvents: Experimental Studies of Reorganization Energies and Solvation Dynamics. *J. Phys. Chem* **1996,** *100*, 10337-10354.
64. Piechota, E. J.; Meyer, G. J., Introduction to Electron Transfer: Theoretical Foundations and Pedagogical Examples. *J. Chem. Ed.* **2019,** *96*, 2450-2466.
65. Caldeweyher, E.; Mewes, J.-M.; Ehlert, S.; Grimme, S., Extension and Evaluation of the D4 London-Dispersion Model for Periodic Systems. *Phys. Chem. Chem. Phys.* **2020,** *22*, 8499-8512.
66. Gillett, A. J.; Tonnelé, C.; Londi, G.; Ricci, G.; Catherin, M.; Unson, D. M. L.; Casanova, D.; Castet, F.; Olivier, Y.; Chen, W. M*., et al.*, Spontaneous Exciton Dissociation Enables Spin State Interconversion in Delayed Fluorescence Organic Semiconductors. *Nature Comm.* **2021,** *12*, 6640.
67. Epifanovsky, E.; Gilbert, A. T. B.; Feng, X.; Lee, J.; Mao, Y.; Mardirossian, N.; Pokhilko, P.; White, A. F.; Coons, M. P.; Dempwolff, A. L*., et al.*, Software for the Frontiers of Quantum Chemistry: An Overview of Developments in the Q-Chem 5 Package. *J. Chem. Phys.* **2021,** *155*, 084801.
68. Lowry, M. S.; Goldsmith, J. I.; Slinker, J. D.; Rohl, R.; Pascal, R. A.; Malliaras, G. G.; Bernhard, S., Single-Layer Electroluminescent Devices and Photoinduced Hydrogen Production from an Ionic Iridium(Iii) Complex. *Chem. Mater.* **2005,** *17*, 5712-5719.
69. Wehlin, S. A. M.; Troian-Gautier, L.; Sampaio, R. N.; Marcélis, L.; Meyer, G. J., Ter-Ionic Complex That Forms a Bond Upon Visible Light Absorption. *J. Am. Chem. Soc.* **2018,** *140*, 7799-7802.
70. Troian-Gautier, L.; Beauvilliers, E. E.; Swords, W. B.; Meyer, G. J., Redox Active Ion-Paired Excited States Undergo Dynamic Electron Transfer. *J. Am. Chem. Soc.* **2016,** *138*, 16815-16826.
71. Maurer, A. B.; Meyer, G. J., Stark Spectroscopic Evidence That a Spin Change Accompanies Light Absorption in Transition Metal Polypyridyl Complexes. *J. Am. Chem. Soc.* **2020,** *142*, 6847-6851.
72. Maurer, A. B.; Piechota, E. J.; Meyer, G. J., Excited-State Dipole Moments of Homoleptic [Ru(Bpy′)3]2+ Complexes Measured by Stark Spectroscopy. *J. Phys. Chem. A* **2019,** *123*, 8745-8754.

For TOC Use Only